

# Harmonic Convolutional Networks based on Discrete Cosine Transform

Matej Ulicny, Vladimir A. Krylov, and Rozenn Dahyot

**Abstract**—Convolutional neural networks (CNNs) learn filters in order to capture local correlation patterns in feature space. In this paper we propose to revert to learning combinations of preset spectral filters by switching to CNNs with harmonic blocks. We rely on the use of the Discrete Cosine Transform (DCT) filters which have excellent energy compaction properties and are widely used for image compression. The proposed harmonic blocks rely on DCT-modeling and replace conventional convolutional layers to produce partially or fully harmonic versions of new or existing CNN architectures. We demonstrate how the harmonic networks can be efficiently compressed in a straightforward manner by truncating high-frequency information in harmonic blocks which is possible due to the redundancies in the spectral domain. We report extensive experimental validation demonstrating the benefits of the introduction of harmonic blocks into state-of-the-art CNN models in image classification, segmentation and edge detection applications.

**Index Terms**—Harmonic Network, Convolutional Neural Networks, Discrete Cosine Transform, Image Classification, Object Detection, Edge Detection.



## 1 INTRODUCTION

CNNs have been designed to take advantage of implicit characteristics of natural images, specifically correlation in local neighborhood and feature equivariance. The wide application of features obtained by convolving images with explicitly defined local filters highlights the shift from the extraction of global information towards local learning.

Standard CNNs rely on the learned convolutional filters that allow them to be adjusted flexibly to the data available. In some cases, however, it may be advantageous to revert to preset filter banks. For instance with limited training data, using a collection of preset filters can help in avoiding overfitting and in reducing the computational complexity of the system. An example of such networks with preset (wavelet based) filters is the scattering network, which achieved state-of-the-art results in handwritten digit recognition and texture classification [1].

We propose instead to replace the standard convolutional operations in CNNs by harmonic blocks that learn the weighted sums of responses to the Discrete Cosine Transform (DCT) filters, see Fig. 1. DCT has been successfully used for JPEG encoding to transform image blocks into spectral representations to capture the most information with a small number of coefficients [2]. Motivated by frequency separation and energy compaction properties of DCT, the proposed harmonic networks rely on combining responses of window-based DCT with a small receptive field. Our method learns how to optimally combine spectral coefficients at every layer to produce a fixed size representation defined as a weighted sum of responses to DCT filters. The use of DCT filters allows one to easily address the task of model compression. While other works that propose convolutional filters decomposition to

particular basis functions [3], [4] have mostly focused on ability to compress the network, we show furthermore that prior information coming from well chosen filter basis can not only be used for compression but can also speed up training convergence and improve performance.

This paper presents a comprehensive study based on our earlier works [5], [6] on harmonic blocks<sup>1</sup>. In this work we introduce further analysis and substantially expand the experimental validation to include edge and object detection cases that broader demonstrate the benefits of harmonic networks. The relevant background is first presented (Sec. 2) and our harmonic network formulation is then explained in Sec. 3. Our proposed harmonic block acts as elementary unit to encode any neural network. It is extensively validated against state-of-the-art alternatives for image classification (Sec. 4), for object detection and segmentation (Sec. 5), and finally for boundary detection in images (Sec. 6). All our architectures are distinct in our reported results with the name starting with *Harm*. We conclude the paper with some final remarks (Sec. 7). The PyTorch implementations for our harmonic networks are publicly available at <https://github.com/matej-ulicny/harmonic-networks>.

## 2 RELATED WORK

### 2.1 DCT & CNNs

#### 2.1.1 Forensics

Networks trained on DCT coefficients are frequently used in forensics for detection of tampered parts in images. These parts are assumed to have different distribution of DCT coefficients from the rest of the image. A common practice is to classify histograms of preselected DCT coefficients by 1-D convolutional network [7], [8], [9]. Furthermore this task was addressed by a multi-branch 2D CNN [10] trained on feature maps spanned by the first 20 AC coefficients (corresponding to non-zero frequencies in DCT) extracted from JPEG images.

<sup>1</sup>. See result of our harmonic WRN model on STL-10 classification task (<https://paperswithcode.com/sota/image-classification-on-stl-10?p=harmonic-networks-with-limited-training>).

- M. Ulicny and R. Dahyot are with the School of Computer Science and Statistics, Trinity College Dublin, Dublin, Ireland. Email: ulinm@tcd.ie, rozenn.dahyot@tcd.ie
- V. Krylov is with the School of Mathematics, Dublin City University, Dublin, Ireland. Email: vladimir.krylov@dcu.ie

## Harmonic block

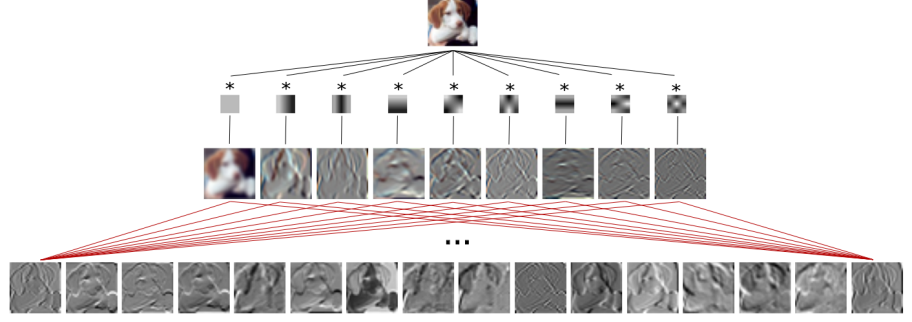
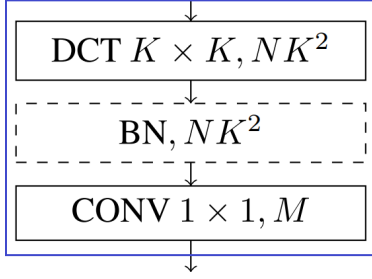


Fig. 1. Left: Design of the harmonic block. Boxes show operation type, size of filter (if applicable) and the number of output channels given the block filter size  $K$ , number of input channels  $N$  and output channels  $M$ . Batch normalization (BN) block is optional. Right: Visualization of the harmonic block applied to an input layer.

### 2.1.2 Object recognition & classification

A number of studies have investigated the use of spectral image representations for object recognition. DCT on small resolution images coupled with coefficient truncation was used to speed up training of fully connected sparse autoencoders [11]. DCT features from the entire image were used to train Radial Basis Function Network for face recognition [12]. A significant convergence speedup and case-specific accuracy improvement have been achieved by applying DCT transform to early stage learned feature maps in shallow CNNs [13] whereas the later stage convolutional filters were operating on a sparse spectral feature representation. In [14], [15] it was demonstrated how DCT coefficients can be efficiently used to train CNNs for classification, where the DCT coefficients can be computed or taken directly from JPEG image format.

## 2.2 Wavelets & CNNs

### 2.2.1 Scattering networks

As an alternative to DCT, scattering Networks [1] are built on complex-valued Morlet wavelets. The scattering networks have its filters designed to extract translation and rotation invariant representations and it was shown to achieve comparable classification accuracy to unsupervised deep learning [16] (*unsupervised* convolutional deep learning algorithms have filters optimized with nonlabeled training data for feature extraction only, before the classifier). The scattering network based on rotation and scale invariant wavelet transform was shown to effectively reduce the input representation while preserving discriminative information for training CNN on image classification [17], [18] and object detection task [19] achieving performance comparable to deeper models. Williams *et al.* [20] have advocated image preprocessing with wavelet transform, but used different CNNs for each frequency subband. Wavelet filters were also used as a preprocessing method prior to NN-based classifier [21], and to enhance edge information in images prior to classification [22].

### 2.2.2 Other spectral based CNNs

Other works have used wavelets in CNN computational graphs. Second order coefficients from Fast Wavelet Transform were used in [23] to design wavelet pooling operator. Similar approach was taken by Ripperl *et al.* who designed spectral pooling [24] based on Fast Fourier Transform of the features and proposing truncation of the high-frequency coefficients. They also proposed to parameterize filters in the Fourier domain to decrease their redundancy

and speed up the convergence when training the network. In both works, the pooled features were recovered with Inverse Fast Wavelet or Inverse Discrete Fourier Transform respectively, thus the CNN still operates in the spatial domain.

To address texture classification, Fujieda *et al.* [25] proposed a Wavelet Convolutional Network that is trained on responses to Haar wavelets and concatenates higher order coefficient maps along with features of the same dimensionality learned from lower-order coefficients. Similar approach is taken by Lu *et al.* [26] that learns from both spatial and spectral information that is decomposed from first layer features. The higher-order coefficients are also concatenated along with the lower dimensional feature maps. However, contrary to our harmonic networks, Wavelet CNNs decompose only the input features and not the features learned at intermediate stages. Robustness to object rotations was addressed by modulating learned filters by oriented Gabor filters [27]. Worrall *et al.* incorporated complex circular harmonics into CNNs to learn rotation equivariant representations [28]. Similarly to our harmonic block, the structured receptive field block [29] learns new filters by combining fixed filters, a set of Gaussian derivatives with considerably large spatial extent. Additionally, Gaussian derivative bases of small spatial extent have been used by Kobayashi to express convolutional filters [30]. DCFNet [3] expresses filters by truncated expansion of Fourier-Bessel basis, maintaining accuracy of the original model while reducing the number of parameters.

## 2.3 Compressing DNNs

Numerous works have focused on compressing the size of neural networks and decreasing the inference and training time. Speedup and memory saving for inference can be achieved by approximating the trained full-rank CNN filters by separable rank-1 filters [31]. Assuming smoothness of learned filters, Frequency-Sensitive Hashed Network (FreshNet) [32] expresses filters by their DCT representation and groups their parameters to share the same value within each group. Wang *et al.* [33] relaxes this constrain to express each weight by its residual from the cluster center. Weights in this form were quantized and transformed via Huffman coding (used for JPEG compression) for limiting storage. Convolution was performed in the frequency domain to reduce the computational complexity. Han *et al.* [34] compressed networks by pruning, clustering and quantizing weights which are consequently fine-tuned. It has been shown [35] that a model complexity can be adjusted during the training time: increased

via introduction of new filters by rotating and applying noise to existing ones, and reduced by clustering to selectively decrease their redundancy.

### 3 HARMONIC NETWORKS

A convolutional layer extracts correlation of input patterns with locally applied learned filters. The idea of convolutions applied to images stems from the observation that pixels in local neighborhoods of natural images tend to be strongly correlated. In many image analysis applications, transformation methods are used to decorrelate signals forming an image [36]. In contrast with spatial convolution with learned kernels, this study proposes feature learning by weighted combinations of responses to predefined filters. The latter extracts harmonics from lower-level features in a region. The use of well selected predefined filters allows one to reduce the impact of overfitting and decrease computational complexity. In this work we focus on the use of DCT as the underlying transformation.

#### 3.1 Discrete Cosine Transform

DCT is an orthogonal transformation method that decomposes an image to its spatial frequency spectrum. In continuous form, a 2D signal is projected to a sum of sinusoids with different frequencies. The contribution of each sinusoid towards the whole signal is determined by its coefficient calculated during the transformation. DCT is also a separable transform and due to its energy compaction properties on natural images [36] it is commonly used for image and video compression in widely used JPEG and MPEG formats. Karhunen-Loève transform (KLT) is considered to be optimal in signal decorrelation, however it transforms signal via unique basis functions that are not separable and need to be estimated from the data. On locally correlated signals such as natural images DCT was shown to closely approximate KLT [37].

The literature provides several distinct definitions of DCT. We will rely on the most common formulation, DCT-II, which is computed on a 2-dimensional grid of the image  $X$  of size  $A \times B$  representing the image patch with 1 pixel discretisation step as

$$Y_{u,v} = \sum_{x=0}^{A-1} \sum_{y=0}^{B-1} \sqrt{\frac{\alpha_u}{A}} \sqrt{\frac{\alpha_v}{B}} X_{x,y} \times \cos \left[ \frac{\pi}{A} \left( x + \frac{1}{2} \right) u \right] \cos \left[ \frac{\pi}{B} \left( y + \frac{1}{2} \right) v \right]. \quad (1)$$

This reports the DCT coefficient  $Y_{u,v}$  representing the transformation of the input with sinusoids at frequency  $u$  and  $v$  in horizontal and vertical orientations, respectively. Basis functions are typically normalized with factors  $\alpha_u = 1$  (resp.  $\alpha_v = 1$ ) when  $u = 0$  (resp. when  $v = 0$ ) and  $\alpha_u = 2$  (resp.  $\alpha_v = 2$ ) otherwise to ensure their orthonormality.

#### 3.2 Harmonic blocks

A harmonic block is proposed to replace a conventional convolutional operation and relies on processing the data in two stages (see Fig. 1). Firstly, the input features undergo harmonic decomposition by a transformation method. Conceptually, various transformation methods can be used e.g. wavelets, derivatives of Gaussians, etc. In this study we focus on window-based DCT. In the second stage, the transformed signals are combined by learned weights. The fundamental difference from standard convolutional network is

that the optimization algorithm is not searching for filters that extract spatial correlation, rather learns the relative importance of preset feature extractors (DCT filters) at multiple layers.

Harmonic blocks are integrated as a structural element in the existing or new CNN architectures. We thus design harmonic networks that consist of one or more harmonic blocks and, optionally, standard learned convolutions and fully-connected layers, as well as any other structural elements of a neural net. Spectral decomposition of input features into block-DCT representation is implemented as a convolution with DCT basis functions. A 2D kernel with size  $K \times K$  is constructed for each basis function, comprising a filter bank of depth  $K^2$ , which is separately applied to each of the input features. Convolution with the filter bank isolates coefficients of DCT basis functions to their exclusive feature maps, creating a new feature map per each channel and each frequency considered. The number of operations required to calculate this representation can be minimized by decomposing 2D DCT filter into two rank-1 filters and applying them as separable convolution to rows and columns sequentially. Despite the operation being computationally cheaper compared to dense convolutions, the spectral decomposition upsamples the number of intermediate features by  $K^2$  factor, thus notably increasing the corresponding memory requirements.

Each feature map  $h^l$  at depth  $l$  is computed as a weighted linear combination of DCT coefficients across all input channels  $N$ :

$$h^l = \sum_{n=0}^{N-1} \sum_{u=0}^{K-1} \sum_{v=0}^{K-1} w_{n,u,v}^l \psi_{u,v} * h_n^{l-1} \quad (2)$$

where  $\psi_{u,v}$  is a  $u, v$  frequency selective DCT filter of size  $K \times K$ ,  $*$  the 2-dimensional convolution operator and  $w_{n,u,v}^l$  is learned weight for  $u, v$  frequency of the  $n$ -th feature. The linear combination of spectral coefficients is implemented via a convolution with  $1 \times 1$  filter that scales and sums the features, see Fig. 1. Since the DCT is a linear transformation, backward pass through the transform layer is performed similarly to a backward pass through a convolution layer. Harmonic blocks are designed to learn the *same* number of parameters as their convolutional counterparts. Such blocks can be considered a special case of depth-separable convolution with predefined spatial filters.

DCT is distinguished by its energy compaction capabilities which typically results in higher filter responses in lower frequencies. The undesirable behaviour of relative loss of high frequency information can be efficiently handled by normalizing spectrum of the input channels. This can be achieved via batch normalization that adjusts per frequency mean and variance prior to the weighted combination. The spectrum normalization transforms Eq. (2) into:

$$h^l = \sum_{n=0}^{N-1} \sum_{u=0}^{K-1} \sum_{v=0}^{K-1} w_{n,u,v}^l \frac{\psi_{u,v} * h_n^{l-1} - \mu_{n,u,v}^l}{\sigma_{n,u,v}^l}, \quad (3)$$

with parameters  $\mu_{n,u,v}^l$  and  $\sigma_{n,u,v}^l$  estimated per input batch.

#### 3.3 Harmonic Network Compression

The JPEG compression encoding relies on stronger quantisation of higher frequency DCT coefficients. This is motivated by the human visual system which often prioritises low frequency information over high frequencies. We propose to employ similar idea in the harmonic network architecture. Specifically, we limit the visual spectrum of harmonic blocks to only several most informative low frequencies, which results in a reduction of number of

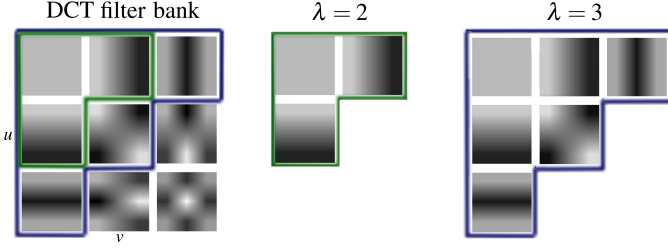


Fig. 2.  $3 \times 3$  DCT filter bank employed in the harmonic networks and its compression.

parameters and operations required at each block. The coefficients are (partially) ordered by their relative importance for the visual system in triangular patterns starting at the most important zero frequency at the top-left corner, see Fig. 2. We limit the spectrum of considered frequencies by hyperparameter  $\lambda$  representing the number of levels of coefficients included perpendicularly to the main diagonal direction starting from zero frequency: DC only for  $\lambda = 1$ , three coefficients used for  $\lambda = 2$ , and six coefficients used for  $\lambda = 3$ . Fig. 2 illustrates filters used at various levels assuming a  $3 \times 3$  receptive field. Thus, reformulating convolutional layers as harmonic allows one to take advantage of this natural approach to model compression, and in doing also introduce additional regularization into the model. The empirical impact of harmonic model compression will be investigated in more detail in the experiments below.

### 3.4 Overlapping cosine transform

DCT computed on overlapping windows is also known as Lapped Transform or Modified DCT (MDCT), related to our harmonic block using strides. The overlapped DCT has a long history in signal compression and reduces artefacts at window edges [38]. Dedicated strategies for efficient computations have been proposed [38], including algorithms and hardware optimisations.

DCT transform is equivalent to the discrete Fourier transform of real valued functions with even symmetry within twice larger window. DCT lacks imaginary component given by the sine transform of real valued odd functions. However, harmonic block allows convolution with DCT basis with arbitrary stride creating redundancy in the representation. Ignoring the boundary limitations, sine filter basis can be devised by shifting the cosine filters. Given the equivariant properties of convolution, instead of shifting the filters the same result is achieved by applying original filters to the shifted input. Considering DCT-II formulation for 1D signal  $X$  with  $N$  values, the DCT coefficient at frequency  $k$  is:

$$F_k = \sum_{n=0}^{N-1} X_n \cos \left[ \frac{\pi}{N} \left( n + \frac{1}{2} \right) k \right] \quad (4)$$

a corresponding sine transform is

$$G_k = \sum_{n=0}^{N-1} X_n \sin \left[ \frac{\pi}{N} \left( n + \frac{1}{2} \right) k \right] \quad (5)$$

which is equivalent to

$$G_k = \sum_{n=0}^{N-1} X_n \cos \left[ \frac{\pi}{2} + 2\pi z - \frac{\pi}{N} \left( n + \frac{1}{2} \right) k \right]. \quad (6)$$

The shift given by  $\pi/2 + 2\pi z$  for any  $z \in \mathbb{Z}$  can be directly converted to shift in pixels applied to data  $X$ . After simplification, sine transform can be expressed as

$$G_k = \sum_{n=0}^{N-1} X_n \cos \left[ \frac{\pi}{N} \left( n - \frac{N(1+4z)}{2k} + \frac{1}{2} \right) k \right] \quad (7)$$

which is equivalent to the cosine transform of the image shifted by  $\delta = N(1+4z)/2k$  defined in (8).

$$F_k[\delta] = \sum_{n=0}^{N-1} X_{n+\frac{N(1+4z)}{2k}} \cos \left[ \frac{\pi}{N} \left( n + \frac{1}{2} \right) k \right]. \quad (8)$$

This value represents the stride to shift the cosine filters to capture correlation with sine function.

In other words, by applying DCT with a certain stride it is possible to obtain the feature representation as rich as that obtained with the full Fourier transform.

### 3.5 Computational Requirements

Harmonic blocks are designed to learn the same number of parameters as their convolutional counterparts. Requirements for the DCT transform scale linearly with the number of input channels and result in a modest increase to the theoretical number of operations. Standard convolutional layer used in many popular architectures that has  $N$  input and  $M$  output channels with a kernel size  $K \times K$  learns  $NMK^2$  parameters and performs  $NMK^2AB$  operations if the filter is applied  $A$  and  $B$  times in particular directions. Harmonic block with  $K^2$  transformation filters of size  $K \times K$  upsamples representation to  $NK^2$  features and then learns one weight for each upsampled-output feature pair hence  $NK^2M$  weights. Transform of an  $A \times B$  feature set costs  $NK^2K^2AB$  on top of weighted combination  $NK^2MAB$  that matches number of multiply-add operations of  $K \times K$  convolution. The total number of operations is thus  $NK^2AB(M + K^2)$ . The theoretical number of multiply-add operations over the standard convolutional layer increases by a factor of  $K^2/M$ . If we assume truncated spectrum (use of  $\lambda \leq K$ ) given by  $P = \lambda(\lambda + 1)/2$  filters, proportion of operations becomes  $P/K^2 + P/M$ .

While keeping the number of parameters intact, a harmonic block requires additional memory during training and inference to store transformed feature representation. In our experiments with WRN models (Sec.4.2), the harmonic network trained with full DCT spectrum requires almost 3 times more memory than the baseline. This memory requirement can be reduced by using the DCT spectrum compression.

Despite the comparable theoretical computational requirements, the run time of harmonic networks is larger compared to the baseline models, at least twice slower (on GPU) in certain configurations. This effect is due to the design of harmonic block that replaces a single convolutional layer by a block of 2 sequential convolutions (with individual harmonic filters and  $1 \times 1$  convolution). Most blocks do not need BN between the convolutions and thus represent a combined linear transformation. The associativity property of convolutions allows one to reformulate the standard harmonic block defined above so that the DCT transform and

**Algorithm 1:** Memory efficient harmonic block

---

**Input:**  $h^{l-1}$   
 Define updates  $g \in \mathcal{R}^{M \times N \times K \times K}$ ;  
**for**  $m \in \{0..M-1\}$  **do**  
   **for**  $n \in \{0..N-1\}$  **do**  
      $g_{m,n}^l \leftarrow \sum_{u=0}^{K-1} \sum_{v=0}^{K-1} w_{m,n,u,v} \psi_{u,v}$ ;  
   **end**  
**end**  
 $h^l \leftarrow g^l * h^{l-1}$ ;  
**Output:**  $h^l$

---

linear combination can be effectively merged into a single linear operation:

$$\begin{aligned}
 h^l &= \sum_{n=0}^{N-1} \sum_{u=0}^{K-1} \sum_{v=0}^{K-1} w_{n,u,v} (\psi_{u,v} * h_n^{l-1}) \\
 &= \sum_{n=0}^{N-1} \left( \sum_{u=0}^{K-1} \sum_{v=0}^{K-1} w_{n,u,v} \psi_{u,v} \right) * h_n^{l-1}
 \end{aligned} \tag{9}$$

In other words, equivalent features can be obtained by factorizing filters as linear combination of DCT basis functions. We thus propose a faster Algorithm 1 that is a more memory efficient alternative to the standard two-stage harmonic block formulation.

This reformulation is similar to structured receptive field [29] utilizing different basis functions. The Algorithm 1 overhead in terms of multiply-add operations with respect to the standard convolutional layer is only  $K^2/AB$ , where the input image size for the block is  $A \times B$ . The experimental performance of the algorithm is evaluated in Section 4.2.

## 4 IMAGE CLASSIFICATION

The performance of the harmonic networks is assessed for image classification on small (NORB, Sec. 4.1), medium (CIFAR-10 and CIFAR-100, Sec. 4.2) and large (ImageNet-1K, Sec. 4.3) scale datasets. We consider a simple 2-layer CNN for the NORB dataset, and two typologies of Residual Networks [39], [40] for other datasets as the baselines for substituting the standard convolution operations with harmonic blocks.

### 4.1 Small NORB dataset

The small NORB dataset [41] was intended for a task of 3D object recognition from shape. It is a synthetic set of  $96 \times 96$  binocular images of 50 toys sorted into 5 classes (four-legged animals, human figures, airplanes, trucks, and cars), captured under different lighting and pose conditions (i.e. 18 different angles, 9 elevations and 6 lighting conditions induced by combining different light sources, see example images in Figure 3). Training and test sets used in our experiments are retained original [41]<sup>2</sup>.

We show first that harmonic networks outperform standard and state-of-the-art CNNs in both accuracy and compactness (c.f. Section 4.1.1) and also illustrate how Harmonic networks can be naturally resilient to unseen illumination changes without resorting to using data augmentation (Sec. 4.1.2).



Fig. 3. Images [41] of an object at two elevations captured with each of the six lighting conditions 0-5 ordered from left to right.

TABLE 1

Models used in NORB experiments. Each row shows operation performed at a given spatial resolution. Convolution and harmonic are denoted as {conv, harm} M,K×K/S with M output features, kernel size K and stride S; similarly for pooling K×K/S and fully connected layers fc M.

Res.	CNN2	CNN3	Harm-Net 2   3   4
96x96	conv 32,5x5/2	conv 32,5x5/2	harm 32,4x4/4
48x48	pool 3x3/2	conv 64,3x3/2	
24x24	conv 64,3x3/2	pool 2x2/2	harm 64,3x3/2
12x12	pool 3x3/2	conv 128,3x3/2	pool 3x3/2
6x6	fc 1024	pool 2x2/2	-   harm 128,3x3/2   harm 128,3x3/2
3x3		fc 1024	fc 1024   fc 1024   harm 1024,3x3/3
1x1	dropout 0.5	dropout 0.5	dropout 0.5
1x1	fc 5	fc 5	fc 5

#### 4.1.1 Comparisons CNN vs. Harmonic Nets

**Baseline architectures.** The baseline CNN network is selected after an extensive hyper-parameter search. The network (CNN2) consists of 2 convolution layers with 32 5×5 and 64 3×3 filter banks respectively, a fully connected layer with 1024 neurons followed by a softmax classifier. Filters are applied with stride 2 and features are subsampled by overlapping max-pooling. All hidden layer responses are batch normalized and rectified by ReLU. We also use a slightly deeper network (CNN3) with an additional convolutional layer preceding the first pooling. Details of the architectures are summarised in Table 1.

**Optimisation.** The baseline CNNs are trained with stochastic gradient descent for 200 epochs with momentum 0.9. The initial learning rate 0.01 is decreased by factor 10 every 50 epochs. The network is trained with batches of 64 stereo image pairs and each pair is padded with zeros 5 pixels on each side and a random crop of 96×96 pixels is fed to the network. The optimization is regularized by dropout (p=0.5) on the fully connected layer and the weight decay is set to 0.0005.

**Harmonic Networks architectures.** Several versions of harmonic networks are considered (Tab. 1), by substituting the first, first two or all three of CNN2 and CNN3 convolution layers by harmonic blocks. Furthermore, the first fully-connected layer can be transformed to a harmonic block taking global DCT transform of the activations. The first harmonic block uses 4×4 DCT filters applied without overlap, the further blocks mimic their convolutional counterparts with 3×3 kernels and stride 2. Standard max or average pooling operator is applied between blocks. Using larger input receptive field realized by DCT transform did not provide any notable advantage.

**Performance evaluation.** The baseline CNN architecture shows poor generalization performance in early stages of training. The performance on a test set stabilizes only after the third decrease of the learning rate, see Fig. 4. Baseline CNN achieved mean error  $3.48\% \pm 0.50$  from 20 trials, while CNN utilizing harmonic blocks

2. <https://cs.nyu.edu/~yiclab/data/norb-v1.0-small/>



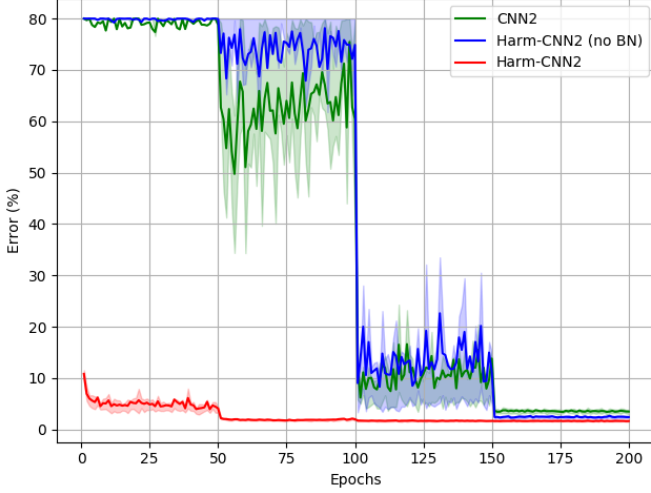


Fig. 4. Mean classification error on small NORB test set. Weak generalization of CNN (green) and harmonic network (blue) is observed during the early stages of training. Filled areas (best seen in color) show 50% empirical confidence intervals from 20 runs. Batch normalization of DCT spectrum (first block) significantly speeds up convergence of harmonic network (red).

TABLE 2

Introduction of harmonic blocks into the baseline architectures and the respective errors on small NORB dataset.

Harmonic layers	Architecture	Pooling type	Error %
	CNN2	overlap max	$3.48 \pm 0.50$
1	Harm-CNN2*	max (no BN)	$2.40 \pm 0.39$
1	Harm-CNN2*	max	$1.63 \pm 0.19$
1	Harm-CNN2*	avg	$1.67 \pm 0.25$
1,2	Harm-Net2	max	$1.60 \pm 0.18$
1,2	Harm-Net2	avg	$1.56 \pm 0.18$
	CNN3	max	$3.43 \pm 0.31$
	CNN3	overlap max	$3.89 \pm 0.65$
1	Harm-CNN3*	overlap avg (no BN)	$2.56 \pm 0.39$
1	Harm-CNN3*	overlap max	$1.16 \pm 0.15$
1	Harm-CNN3*	overlap avg	$1.14 \pm 0.20$
1,2	Harm-CNN3*	overlap max	$1.21 \pm 0.17$
1,2	Harm-CNN3*	overlap avg	$1.15 \pm 0.17$
1,2,3	Harm-Net3	overlap max	$1.18 \pm 0.16$
1,2,3	Harm-Net3	overlap avg	$1.15 \pm 0.22$
1,2,3,4	Harm-Net4	overlap avg	<b><math>1.10 \pm 0.16</math></b>

\*These architectures are constructed by taking the upper part from the Harm-Net and the bottom from CNN baseline with the same number of conv/harm layers.

without explicit normalization of harmonic responses exhibits similar behavior resulting in better final solution of  $2.40\% \pm 0.39$ . Normalizing DCT responses of input channels at the first block prevents harmonic network from focusing too much on pixel intensity, allows using  $10\times$  higher learning rate, significantly speeds up convergence, improves performance and stability.

We observe the average pooling to work well in combination with harmonic blocks. Error of  $1.14\% \pm 0.20$  is achieved by a hybrid model with one harmonic block followed by 2 standard convolutional layers using overlapping average pooling between them. A variant with 3 harmonic blocks and the same configuration performs comparably with  $1.15\% \pm 0.22$  error (c.f. Tab. 2). The best result was obtained by the model with 3 harmonic blocks replacing the convolutional layers and the fully-connected layer transformed into harmonic block, misclassifying only  $1.10\% \pm 0.16$  of test samples.

TABLE 3

Comparison with the state-of-the-art on small NORB dataset, showing the proposed method outperforms other reported results.

Method	Parameters	Error %
CNN with input filter [43]	2.7M	$2.53 \pm 0.40^*$
Nonlinear SLPP [44]		1.5*
CapsNet [42] multi-crop	310K	1.4*
CapsNet [42] small	68K	2.2*
Harm-Net4	1.28M	<b><math>1.10 \pm 0.16</math></b>
Harm-Net4, fc M=32, no dropout	131K	$1.17 \pm 0.20$
Harm-Net4, fc M=32, no dropout, $\lambda = 3$	88K	$1.34 \pm 0.21$
Harm-Net4, fc M=32, no dropout, $\lambda = 2$	45K	$1.64 \pm 0.22$

\*scores reported by the authors of the corresponding papers.

**Comparison with state-of-the-art.** Table 3 shows that these results surpass all previously reported error rates for this dataset to the best of our knowledge. The capsule network [42] claims 1.4% error rate however estimated under different evaluation protocol, where testing images are resized to  $48 \times 48$  and prediction for multiple crops of size  $32 \times 32$  is averaged. The best reported result for a CNN [43]  $2.53\% \pm 0.40$  uses wider CNN architecture and four additional input channels derived from original input via contrast-extractive filters.

**Harmonic network compression.** We further proceed to designing a very compact version of Harm-Net4 (cf. Table 3). To do so, the fully connected layer is reduced to only 32 neurons and the dropout is omitted. The modified network reaches  $1.17\% \pm 0.20$  error and has 131k parameters. When applying compression with  $\lambda = 3$  the network reaches  $1.34\% \pm 0.21$  and requires less than 88k parameters<sup>3</sup>. By applying  $\lambda = 2$  the total is less than 45k parameters. This model uses non-overlapping pooling to preserve more of limited high-frequency information. Error of  $1.64\% \pm 0.22$  is achieved on the test set, in contrast with small capsule network [42] with 68k parameters scoring 2.2%.

#### 4.1.2 Harmonic Networks for illumination changes

Spectral representation of input data has a few interesting properties. Average feature intensity is captured into DC coefficient, while other (AC) coefficients capture signal structure. DCT representation has been successfully used [12] to build illumination invariant representation. This gives us strong motivation to test illumination invariance properties of harmonic networks and to compare them with standard CNNs.

Objects in the small NORB dataset are normalized and are presented with their shadows over uniform background. The six lighting conditions are obtained by various combination of up to 4 fixed light sources at different positions and distances from the objects.

Usual approaches to reduce sensitivity to lighting conditions include image standardization with ZCA whitening [45] or illumination augmentation. Data augmentation is the standard approach in CNNs for compensating the lack of variability in the available training data. Brightness and contrast manipulations encourage the network to focus on features that are independent of the illumination and may as well generate images resembling lighting conditions in the target domain. Contrary to these methods in our approach we achieve the same effect by removing the filter corresponding to the DC component from the first harmonic block.

3. In this particular setting, the first harmonic block manipulates  $4 \times 4$  filters and uses  $\lambda_{4 \times 4} = \lambda_{3 \times 3} + 1$ .

TABLE 4

Means of classification error over 10 runs over the test images captured in unseen illumination conditions using small NORB dataset.

Augmentation Lighting Condition	None		Brightness & contrast	
	CNN	Harmonic	CNN	Harmonic
Bright	26.3±2.6	10.2±0.4	17.6±0.7	9.4±0.7
Standard	30.2±1.8	18.0±1.9	22.48±1.1	15.5±1.1
Dark	31.2±1.8	18.9±1.2	20.1±1.3	14.5±1.4

Such network is invariant towards global additive changes in pixel intensity by definition.

**Set-up.** The dataset is split into 3 parts based on lighting conditions during image capturing: the bright images (conditions 3,5) dark images (conditions 2,4) and images under standard lighting conditions (0,1) illustrated on Fig. 3. The models are trained (with and without data augmentation) only on data from one split and tested on images from the other two splits that contain unseen lighting conditions.

**Performance evaluation.** Classification errors of the best CNN and harmonic network architectures are reported in Table 4 on the test images (unseen illumination conditions). Harmonic networks consistently achieve lower error under various unseen lighting conditions in comparison to baseline CNNs, with and without random brightness and contrast (only for dark images) data augmentation.

## 4.2 CIFAR-10/100 datasets

The second set of experiments is performed on popular benchmark datasets of small natural images CIFAR-10 and CIFAR-100. Images have three color channels and resolution of 32x32 pixels. The dataset is split into 50k images for training and 10k for testing. Images have balanced labeling, 10 classes in CIFAR-10 and 100 in CIFAR-100.

**Baseline.** For experiments on CIFAR datasets we adopt WRNs [40] with 28 layers and width multiplier 10 (WRN-28-10) as the main baseline. These improve over the standard ResNets by using much wider residual blocks instead of extended depth. Model design and training procedure are kept unchanged as in the original paper. Harmonic WRNs are constructed by replacing convolutional layers by harmonic blocks with the same receptive field, preserving batch normalization and ReLU activations in their original positions after every block.

**Results.** We first investigate whether the WRN results can be improved if trained on spectral information, i.e. when replacing only the first convolutional layer preceding the residual blocks in WRN by a harmonic block with the same receptive field (Harm1-WRN). The network learns more useful features if the RGB spectrum is explicitly normalized by integrating the BN block as demonstrated in Fig. 1, surpassing the classification error of the baseline network on both CIFAR-10 and CIFAR-100 datasets, see Table 5. We then construct a fully harmonic WRN (denoted as Harm-WRN) by replacing all convolutional layers with harmonic blocks, retaining the residual shortcut projections unchanged. *Zagoruyko et al.* [40] demonstrated how dropout blocks placed inside residual blocks between convolutional layers can provide extra regularization when trained on spatial data [40]. We have observed a similar effect when training on spectral representations, therefore we adopt dropout between harmonic

TABLE 5

Settings and median error rates (%) out of 5 runs achieved by WRNs and their harmonic modifications on CIFAR datasets. Number of parameters reported for CIFAR-10.

Method	Dropout	Parameters	CIFAR-10	CIFAR-100
WRN-28-10 [40]	✓	36.5M	3.91	18.75
Harm1-WRN-28-10 (no BN)		36.5M	4.10	19.17
Harm1-WRN-28-10		36.5M	3.90	18.80
Harm1-WRN-28-10	✓	36.5M	<b>3.64</b>	<b>18.57</b>
Harm-WRN-28-10	✓	36.5M	3.86	<b>18.57</b>
Harm-WRN-28-10, $\lambda = 3$	✓	24.4M	3.84	18.58
Harm-WRN-28-10, $\lambda = 2$	✓	12.3M	4.25	19.97
Harm-WRN-28-10, progr. $\lambda$		15.7M	3.93	19.04
Gabor CNN 3-28 [27]		17.6M	3.88*	20.13*
WRN-28-8 [40]	✓	23.4M	4.01	19.38
WRN-28-6 [40]	✓	13.1M	4.09	20.17

\*scores reported by [27].

blocks. The harmonic network outperforms the baseline WRN, see Table 5. Based on this empirical evidence we always employ BN inside the first harmonic block.

Analysis of fully harmonic WRN weights learned with 3x3 spectrum revealed that the deeper network layers tend to favour low-frequency information over high frequencies when learning representations. Relative importance of weights corresponding to different frequencies shown in Fig. 5 motivates truncation of high-frequency coefficients for compression purposes. While preserving the input image spectrum intact, we train the harmonic networks on limited spectrum of hidden features for  $\lambda=2$  and  $\lambda=3$  using 3 and 6 DCT filters for each feature, respectively. To assess the loss of accuracy associated with parameter reduction we train baselines with reduced widths having comparable numbers of parameters: WRN-28-8 and WRN-28-6, see Fig. 6. Fully harmonic WRN-28-10 with  $\lambda=3$  has comparable error to the network using the full spectrum and outperforms the larger baseline WRN-28-10, showing almost no loss in discriminatory information. On the other hand Harm-WRN-28-10 with  $\lambda=2$  is better on CIFAR-100 and slightly worse on CIFAR-10 compared to the similarly sized WRN-28-6. The performance degradation indicates that some of the truncated coefficients carry important discriminatory information. Detailed comparison is reported in Table 5.

We further compare the performance of the harmonic version of WRN-28-10 with the Gabor CNN 3-28 [27] that relies on modulating the learned filters with Gabor orientation filters. To operate on a similar model we remove dropouts and reduce complexity by applying progressive  $\lambda$ : no compression for 32x32 feature sizes,  $\lambda=3$  for 16x16, and  $\lambda=2$  for the rest. With a smaller number of parameters the Harm-WRN-28-10 performs similarly

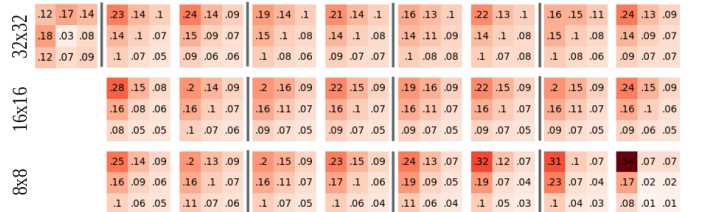


Fig. 5. Distribution of weights (averaged in each layer) assigned to DCT filters in the first harmonic block (left-most) and the remaining blocks in the Harm-WRN-28-10 model trained on CIFAR-10. Vertical lines separate the residual blocks.

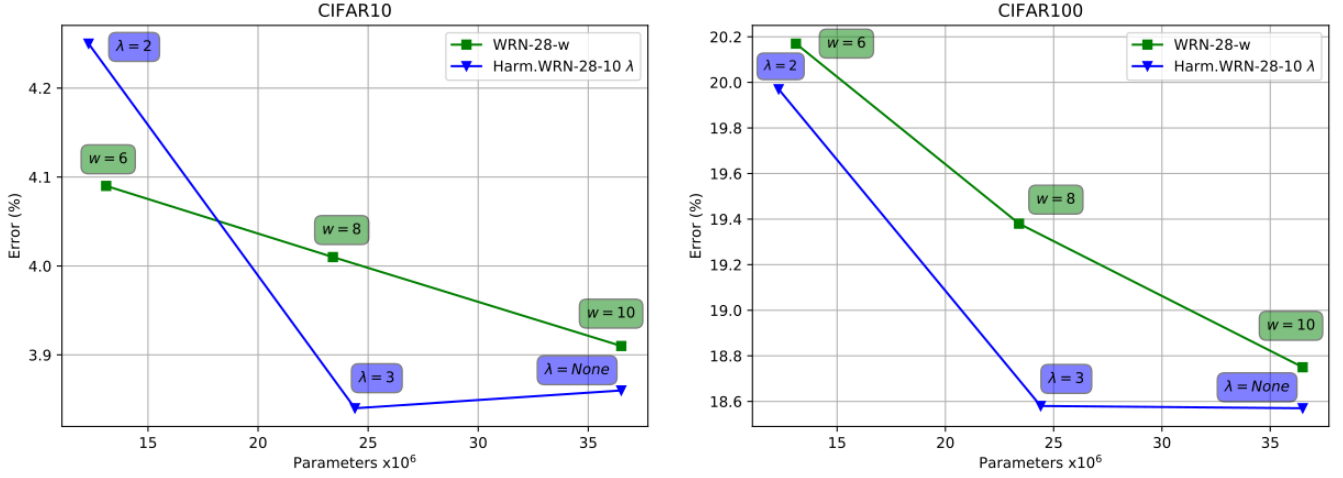


Fig. 6. Decrease of classification error as a function of model size on CIFAR-10 (left) and CIFAR-100 (right). Parameters of harmonic networks are controlled by the compression parameter  $\lambda$ , the WRN baselines by the width multiplier  $w$ .

TABLE 6

Computational requirements of harmonic block implementations on CIFAR-10 with accuracy shown averaged over 5 runs.

Model	GPU memory	Epoch runtime	Error %
WRN-16-8 [40]	2.8GB	45.0s	4.39 $\pm$ 0.14
Harm-WRN-16-8 (standard block)	6.6GB	123.4s	4.44 $\pm$ 0.04
Harm-WRN-16-8 (Alg. 1)	2.9GB	56.8s	4.38 $\pm$ 0.09

on CIFAR-10 and outperforms Gabor CNN on CIFAR-100.

**Harmonic block implementations.** Here we compare the standard harmonic block implementation with its memory efficient version introduced in Algorithm 1, see Table 6. The comparison on CIFAR-10 dataset demonstrates that Algorithm 1 provides similar overall performance but reduces both the runtime and memory requirements by over 50%. We will therefore use solely this implementation of the harmonic block except for the root (first) layers, where this implementation is impossible due to the use of BN.

**Ablation study.** The effect of filter parametrisation by DCT basis is investigated by changing particular layers of WRN-16-4 (without dropout), see Table 7. The effect is measured as a change in standard error over 5 runs. Firstly, the root convolutional layer of WRN is replaced with harmonic block which adds 0.28 absolute improvement over the baseline error 24.07%. Normalization on the DCT responses gains another 0.12. Using the harmonic blocks only in the residual blocks boosts the accuracy of the baseline by 0.85. Replacing the first layer along with the residual blocks

TABLE 7

Modifications of the WRN-16-4 baseline on CIFAR-100: mean classification errors and standard deviations from 5 runs.

Root block	Harmonic root BN	Residual blocks	Error %
			24.07 $\pm$ 0.24
✓			23.79 $\pm$ 0.24
✓	✓		23.67 $\pm$ 0.12
		✓	23.22 $\pm$ 0.28
✓		✓	23.25 $\pm$ 0.25
✓	✓	✓	23.21 $\pm$ 0.11

does not provide any empirical benefit. Adding normalization to the root harmonic block gives only a subtle improvement but decreases the variance by half. These observations correspond to the results obtained on the NORB dataset, see Table 2. We will always be employing BN as part of the root harmonic block.

**Harmonic network compression.** Section 3.3 describes how convolutional filters in certain layer can be approximated with fewer parameters. So far we have only considered uniform coefficient truncation by truncating the same frequencies in all the layers or simple progressive compression. This scheme omits higher number of frequencies in deeper layers, but the same subset of coefficients is used in all harmonic blocks applied to feature maps of particular size. We believe better compression-accuracy trade-off can be achieved by using more elaborate coefficient selection at each layer. In this experiment we start with the WRN-28-10 baseline trained without dropout which has been converted to harmonic WRN-28-10 net (omitting BN in the first harmonic block) by re-expressing each  $3 \times 3$  filter as an optimal combination of DCT basis functions. The first harmonic block is kept intact (no compression in DCT representation), while all other blocks are compressed. We compare three different coefficient selection strategies:

- *Uniform selection:* at every layer the same  $\lambda$  is used;
- *Progressive selection:* the level of compression is selected based on the depth of the layer  $\lambda_{progr} = \max(\alpha, \min(2K - 1, \lfloor T/Depth \rfloor))$  for  $\alpha = 1$  or 2, constant  $T$ , and  $K$  is the size of filter ( $\lambda = 2K - 1$  corresponds to no compression);
- *Adaptive selection:* the compression level is selected adaptively for each layer; the filter is excluded if its  $L1$  compared to the other frequencies in the same layer is too low. Specifically, if  $|w_{i,j}|_1 / \sum_{u,v=0}^{K-1} |w_{u,v}|_1 < T$  then the coefficient is truncated.

The results reported in Fig. 7 confirm the behavior observed above (see Fig. 5), i.e. the high frequencies appear to be more relevant in the early layers of the network compared to deeper layers. The uniform compression fails to adjust and discards the same amount of information in all the layers, and is surpassed



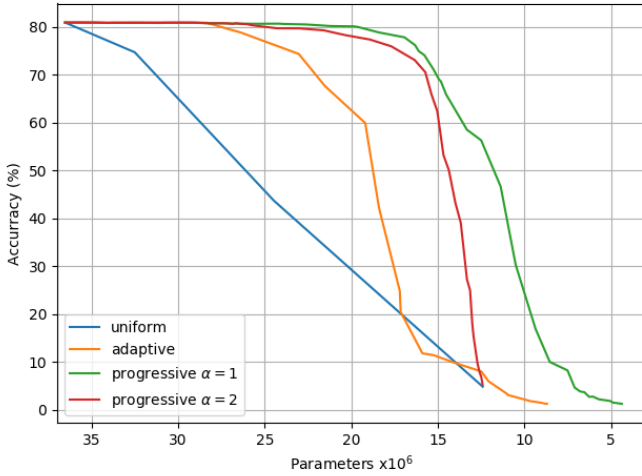


Fig. 7. Accuracy of compressed WRN-28-10 on CIFAR100 using different coefficient truncation strategies.

TABLE 8

Classification errors on ImageNet validation set using central crops after 100 epochs of training.

Model	Parameters	Top-1 %	Top-5 %
VGG16-BN	138.4M	26.33	8.26
Harm-VGG16-BN	138.4M	25.55	8.01
ResNet-50 (no maxpool)	25.6M	23.81	6.98
Harm1-ResNet-50	25.6M	<b>22.97</b>	<b>6.48</b>
Harm-ResNet-50	25.6M	23.11	6.63
Harm-ResNet-50 (avgpool)	25.6M	23.1	6.53
Harm-ResNet-50, progr. $\lambda$	19.7M	23.12	6.61
Harm-ResNet-101	44.5M	21.48	5.75
<b>Benchmarks</b>			
ResNet-50 (maxpool) [46]	25.6M	23.85	7.13
ScatResNet-50 [19]	27.8M	25.5	8.0
JPEG-ResNet-50 [15]	25.6M	23.94	6.98
ResNet-101 (maxpool) [46]	44.5M	22.63	6.44

by other compression strategies. By using progressive or adaptive coefficient selection a model can be compressed by over 20% without loss in accuracy. The best progressive method loses less than 1% of accuracy when compressed by 45% without need for finetuning. Note that frequencies are discarded per layer, selective approach could benefit from more fine-grained compression tailored to individual filters.

### 4.3 ImageNet dataset

In this section we present results obtained on ImageNet-1K classification task. To deploy harmonic networks on large-scale datasets a few adjustments are applied to the harmonic blocks: Firstly, in the absence of BN inside harmonic block we merge the linear operations of feature extraction with DCT basis and weighted combination of responses (use of Algorithm 1). Secondly, we normalize DCT filters by their L1 norm.

ResNet [39] with 50 layers is adopted as the baseline. Following [47] we apply stride on 3x3 convolution instead of the first 1x1 convolution in the block. To reduce memory consumption maxpooling is not used, instead the first convolution layer employs stride 4 to produce equally-sized features; we refer to this modification as ResNet-50 (no maxpool). The following harmonic modifications refer to this baseline without maxpooling after the first layer. Similarly to the above reported CIFAR experiments

TABLE 9

Performance of the converted harmonic networks (error on ImageNet).

Training Epochs	Model	Top-1 %	Top-5 %
full 90	ResNet-50 (no maxpool)	24.36	7.34
full 90	Harm-ResNet-50	23.58	6.91
finetuned 90+5	ResNet-50 $\Rightarrow$ Harm-ResNet-50	24.15	7.15
finetuned 90+5	ResNet-50 $\Rightarrow$ Harm-ResNet-50, progr. $\lambda$	24.60	7.43

we investigate the performance of three harmonic modifications of the baseline: (i) replacing solely the initial 7x7 convolution layer with harmonic block (with BN) with 7x7 DCT filters, (ii) replacing all convolution layers with receptive field larger than 1x1 with equally-sized harmonic blocks, (iii) compressed version of the fully-harmonic network. Each model is trained with stochastic gradient descent with learning rate 0.1, reduced 10 times every 30 epochs reporting the final accuracy at epoch 100. We employ batch size of 256, weight decay 0.0001 and random scale, aspect ratio & horizontal flip augmentation as recommended in [48], producing  $224 \times 224$  crops.

Table 8 reports error rates on ImageNet validation set using central  $224 \times 224$  crops from images resized such that the shorter side is 256. All three harmonic networks have similar performance and improve over the baseline by 0.6–1% in top1 and 0.4–0.6% in top5 accuracy. We observe similar progress of the three modifications during training, see Fig. 8. ResNet-50 architecture has 17 layers with spatial filters which correspond to 11M parameters. We reduce this number by using progressive  $\lambda$  compression:  $\lambda=3$  on  $14 \times 14$  features and  $\lambda=2$  on the smallest feature maps. This reduces the number of weights roughly by half, in total by about 23% of the network size. The compressed network loses almost no accuracy and still clearly outperforms the baseline. It should be noted that harmonic networks without bottleneck residual blocks can be compressed more efficiently. Even with compression the proposed Harm-ResNet-50 confidently outperforms the standard ResNet-50 (maxpool), as well as the more recent ScatResNet-50 [19] and JPEG-ResNet-50 [15], see Table 8. Furthermore, we also observe a substantial improvement of 1.15 in top-1 error % associated with the introduction of harmonic blocks into a deeper ResNet-101 architecture. Note that similarly to ResNet-50 the harmonic version is not using pooling and relies on striding instead to reduce the computational complexity. Finally, Harm-ResNet-50 (avgpool) demonstrates a largely similar quantitative performance to the Harm-ResNet-50, which employs striding after the first layer, at the cost of about 10% computational overheads in training. This experiment further validates the selection of nonpooling-based harmonic architecture as the main model.

We validate the use of harmonic blocks on an architecture without residual connections as well. To this end we employ a VGG16 [49] architecture with BN layers. Harm-VGG16-BN obtained by replacing all convolutional layers by harmonic blocks yields an improvement of approx. 0.8% in top-1 classification error. This demonstrates that the improvement of harmonic networks is not limited to residual connection-based architectures.

Finally, we evaluate the conversion of the weights of a pre-trained non-harmonic network to those of its harmonic version. To this end each learned filter in the pretrained baseline (ResNet-50 without maxpooling after 90 epochs of training) is expressed as a best matching combination of DCT filters. We skip BN inside the first harmonic layer since the related parameters are not available. The direct conversion resulted in the exact same

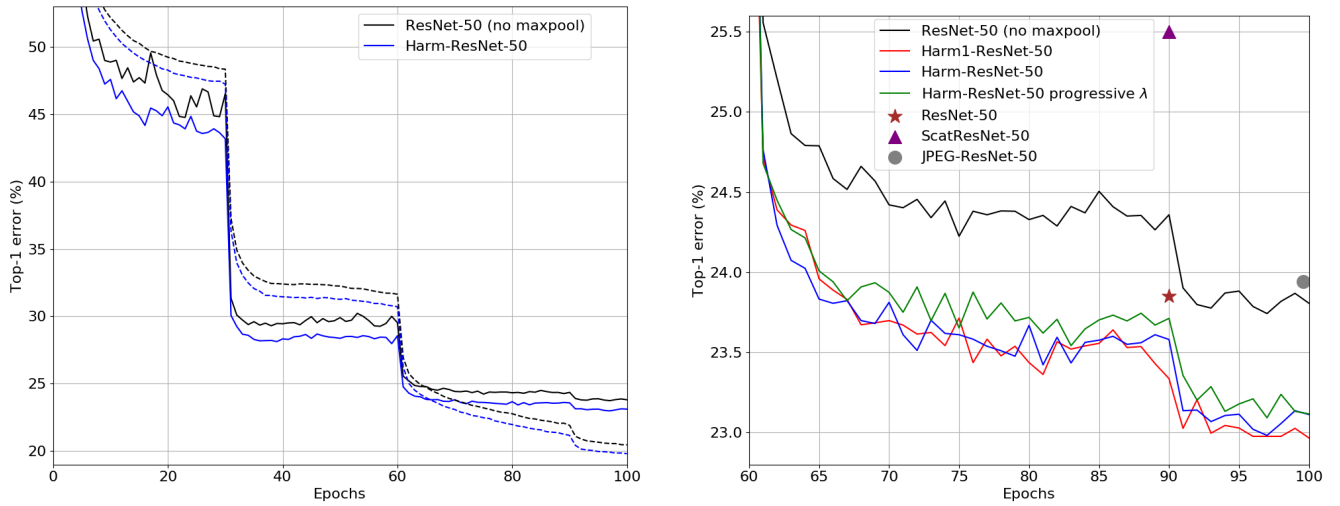


Fig. 8. Training of harmonic networks on ImageNet classification task. Left: comparison with the baseline showing validation error (solid line) and training error (dashed). Right: last 40 epochs of training for all the ResNet-50 based models including scores reported for the benchmark models.

TABLE 10  
SE-ResNeXt networks: harmonic vs. baseline errors and comparison with the state of the art on ImageNet.

Model	Param	224×224			320×320 / 331×331		
		FLOPS	Top-1	Top-5	FLOPS	Top-1	Top-5
<b>ResNeXt-101 (RNx):</b>							
RNX (64x4d) [50]	83.6M	15.5B	20.4	5.3	31.5B	19.1	4.4
SE-RNX(32x4d)	49.0M	8.0B	19.74	4.90	16.3B	18.80	4.19
same, reported in [51]	49.0M	8.0B	19.81	4.96	-	-	-
Harm-SE-RNX(32x4d)	49.0M	8.1B	19.55	4.79	16.5B	18.72	4.23
Harm-SE-RNX(64x4d)	88.2M	15.4B	<b>18.36</b>	<b>4.37</b>	31.4B	<b>17.34</b>	<b>3.71</b>
<b>Benchmarks</b>							
PolyNet [52]	92M	-	-	-	34.7B	18.71	4.25
DualPathNet-131 [53]	79.5M	16.0B	19.93	5.12	32.0B	18.55	4.16
EfficientNet-B4 [54]	19.3M	-	-	-	4.2B	17.4	3.7
SENet-154 [51]	115.1M	20.7B	<b>18.68</b>	<b>4.47</b>	42.3B	17.28	3.79
NASNet-A [55]	88.9M	-	-	-	23.8B	17.3	3.8
AmoebaNet-A [56]	86.7M	-	-	-	23.1B	17.2	3.9
PNASNet [57]	86.1M	-	-	-	25.0B	17.1	3.8
EfficientNet-B7* [54]	66M	-	-	-	37B	<b>15.6</b>	<b>2.9</b>

\*model trained on 600×600 crops.

numerical performance due to the basis properties of DCT. We observe a similar pattern of relative importance of DCT filters to the one reported in Fig. 5. We then finetune the converted model for another 5 epochs with the learning rate of 0.001, which results in the top1 (top5) performance improvement of 0.21% (0.19%) over the pretrained baseline, see Table 9. We also investigate the conversion to a harmonic network with progressive  $\lambda$  compression. After casting the pretrained filters into the available number of DCT filters (from full basis at the early layers to 3 out of 9 filters at the latest layers), the top1 performance degrades by 6.3% due to loss of information. However, if we allow finetuning for as few as 5 epochs the top1 (top5) accuracy falls 0.24% (0.09%) short of the baseline by reducing the number of parameters by 23%. This analysis shows how the harmonic networks can be used to improve the accuracy and / or compress the existing pretrained CNN models.

**Comparison with the cutting-edge techniques.** Here we verify the use of DCT-based harmonic blocks in the more elaborate state-of-the-art models. To this end we modify ResNeXt architec-

ture [50], which is similar to ResNets and uses wider bottleneck and grouped convolution to decrease the amount of FLOPS and the number of parameters. The model is further boosted using several state-of-the-art adjustments: (i) identity mapping in blocks that downsample features are extended by average pooling to prevent information loss; (ii) squeeze and excitation blocks (SE) [51] are used after every residual connection. The network is further regularized by stochastic depth [58] and dropout on the last layer. Training is performed via stochastic gradient descent with learning rate 0.1 and batch size 256, with the former decayed according to one cosine annealing cycle [59]. In addition to mirroring and random crops of size 224, images are augmented with rotations and random erasing [60].

Our ResNeXt modification with 101 layers and 32 groups per 4 convolutional filters in residual block (expressing filters in both standard bases and DCT bases) is trained for 120 epochs. Use of DCT bases provides a subtle improvement over the standard bases. Furthermore we upscale the network to use 64 groups of filters, replace max-pooling in the first layer by increased stride and train this network for 170 epochs. From Table 10 we conclude that our model outperforms all other “handcrafted” architectures that do not use extra training images and performs comparably to the networks of similar complexity found via neural architecture search. It should be noted that these models were also trained on larger image crops than our harmonic network, whereby such training typically improves the accuracy.

## 5 OBJECT DETECTION AND SEGMENTATION

Representations learned from features expressed via harmonic basis are versatile and can serve well for transfer learning. We assess here the performance of harmonic networks in object detection and instance segmentation tasks. The popular single stage RetinaNet [61] and multistage Faster [62] and Mask R-CNN [63] frameworks are built upon our harmonic ResNet backbones. A set of experiments is conducted on the datasets Pascal VOC [64] (Sec. 5.1) and MS COCO [65] (Sec. 5.2).

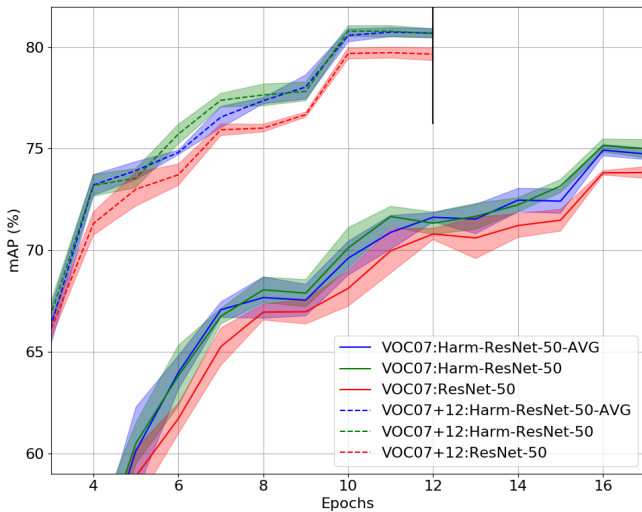


Fig. 9. Training Faster R-CNN with harmonic network backbone on Pascal VOC detection task. Mean average precision on VOC 2007 validation set reported with standard deviation after training on VOC 2007 train (dashed) and VOC 2007 + VOC2012 train (solid) sets.

## 5.1 Pascal VOC

We extend PyTorch implementation provided by Chen et al [66] and train Faster R-CNN model based on our harmonic ResNets with 50 and 101 layers. The first layer and the set of residual blocks used on the highest feature resolution are frozen (not updated) during training. Region proposal network (RPN) is applied on the feature pyramid [67] constructed from the network layers. RPN layers as well as regression and classification heads are randomly initialized and use standard (non-harmonic) convolution/fully connected layers. Images are resized to set their shortest sides at 600 pixels. The Faster R-CNN is trained with the learning rate  $lr = 0.01$  and batch size  $bs = 16$  when the backbones have 50 layers, and  $lr = 0.0075$  and  $bs = 12$  in case of 101 layered configuration. Models are trained on the union of VOC 2007 training and validation sets with about 5000 images for 17 epochs decreasing the learning rate by a multiplicative factor of 0.1 after epoch 15. We train the networks with original and harmonic backbones using the same setting. Additionally, these models are also trained on the combination of training sets of VOC 2007 and VOC 2012, consisting of about 16 500 images, for 12 epochs with learning rate dropped at epoch 9. All models are tested on VOC 2007 test set and the official evaluation metric, the mean average precision (AP), is averaged over 5 runs. Final results are reported in Table 11 for different depths of ResNet backbones, detector architectures and configurations of the datasets. The specific number of epochs and learning schedule were selected

TABLE 11

Mean average precision of Faster R-CNN models after 5 runs on Pascal VOC07 test set. ResNet-101-based models are trained once.

Backbone	Box AP VOC07	Box AP VOC07+12
	17 epochs	12 epochs
ResNet-50	73.8 $\pm$ 0.3	79.7 $\pm$ 0.3
Harm-ResNet-50	<b>75.0 <math>\pm</math> 0.4</b>	<b>80.7 <math>\pm</math> 0.2</b>
Harm-ResNet-50-AVG	74.7 $\pm$ 0.3	<b>80.7 <math>\pm</math> 0.2</b>
ResNet-101	76.1	82.1
Harm-ResNet-101	<b>77.4</b>	<b>82.9</b>

TABLE 12

Mean average precision for different backbones and detector types on MS COCO 2017 validation set. All backbones are transformed to FPNs.

Backbone	Type	Box AP		Mask AP	
		12 epochs	24 epochs	12 epochs	24 epochs
ResNet-50	Faster	36.4	37.7*	-	-
Harm-ResNet-50	Faster	37.2	<b>38.4</b>	-	-
Harm-ResNet-50-AVG	Faster	<b>37.3</b>	38.2	-	-
ResNet-50	Retina	35.6*	36.4*	-	-
Harm-ResNet-50	Retina	36.3	36.8	-	-
Harm-ResNet-50-AVG	Retina	36.3	37.1	-	-
ResNet-101	Faster	38.5	39.3	-	-
Harm-ResNet-101	Faster	<b>39.7</b>	<b>40.3</b>	-	-
ResNet-101	Retina	37.7*	38.1*	-	-
Harm-ResNet-101	Retina	39.0	39.2	-	-
ResNet-50	Mask	37.3*	38.5*	34.2*	35.1*
Harm-ResNet-50	Mask	<b>38.1</b>	<b>38.9</b>	34.7	<b>35.5</b>
Harm-ResNet-50-AVG	Mask	<b>38.1</b>	38.8	<b>35.0</b>	35.4
ResNet-101	Mask	39.4*	40.3*	35.9*	36.5*
Harm-ResNet-101	Mask	<b>40.7</b>	<b>41.5</b>	<b>36.8</b>	<b>37.3</b>

\*scores reported by [66].

to reduce the impact of overfitting. In particular, when trained on VOC07 the larger ResNet-101 and its harmonic version reported a decrease in test performance of approx. 0.5 AP if the training progressed to epoch 20.

From Table 11 we conclude that the models built on our harmonic backbones surpass their conventional convolution-based counterparts in all configurations as well as on both training sets. In Fig. 9 we demonstrate the performance of Faster R-CNN at different stages of training on VOC 2007 and VOC 2007+2012 datasets. Harmonic ResNet-50 with average pooling following the root layer yields comparable results, yet has a mildly higher computational complexity compared to ResNet with striding instead of pooling. We observe a consistent improvement due to the Harmonic architecture: by 1% mAP for ResNet-50 and 0.8% mAP in case of ResNet-101 using the Faster R-CNN architecture.

## 5.2 MS COCO

MS Common Objects in COntext (COCO) dataset poses a greater challenge due to a higher variety of target classes and generally smaller object sizes. Higher input resolution is needed for good accuracy. The networks are trained following the standard procedure, images resized so that their shortest size is 800 pixels. The learning rate is initialized by linear scaling method  $lr = 0.02 \times (bs/16)$  using default hyperparameters set up by Chen et al [66]. Batch size  $bs = 10$  and learning rate  $lr = 0.0125$  are used for shallower models while deeper models required batches of size  $bs = 6$  with the corresponding learning rate of  $lr = 0.0075$ . All models are trained with standard 12 (24) epochs schedules with learning rate decreased by 10 after epochs 8 (16) and 11 (22). Table 12 shows that the use of our harmonic backbones consistently improves both single-stage RetinaNet and multi-stage Faster and Mask R-CNN detectors by 0.7-1.3 AP with identical training procedures employed.

The state-of-the-art detectors rely on the cascade of detection heads with progressively increasing IoU thresholds which refines the bounding boxes and thus improves localization accuracy [68]. In Table 13, we report comparisons achieved with the Cascade R-CNN architecture, trained using the 20-epoch schedule suggested in [68]. The use of our harmonic ResNet-101 provides a 1.0 AP



TABLE 13

Mean average precision on Cascade R-CNN architecture on MS COCO 2017 validation set. All backbones are transformed to FPNs.

Cascade R-CNN Backbone	Type	Box AP 20 epochs	Mask AP 20 epochs
ResNet-101	Faster	42.5*	-
Harm-ResNet-101	Faster	43.5	-
ResNet-101	Mask	43.3*	37.6*
Harm-ResNet-101	Mask	44.3	38.3
ResNet-101	Hybrid	44.9*	39.4*
Harm-ResNet-101	Hybrid	<b>46.0</b>	<b>40.2</b>

\*scores reported by [66].

improvement for object detection similar to Faster & Mask R-CNNs, and it also improves instance segmentation average precision by 0.7 AP (see Table 13). Moreover, a similar improvement of 1.1 AP is observed for hybrid task cascade R-CNN [69] that alters the mask refinement procedure and exploits semantic segmentation information to incorporate additional contextual information.

These experiments on object detection and localization demonstrate that the harmonic versions of the backbones provides a meaningful improvement of about 1.0 AP in terms of both bounding boxes and masks to the state-of-the-art detection architectures. Our harmonic networks retain this improvement from the purely classification task through the transformation to the Feature Pyramid Networks (FPNs).

## 6 BOUNDARY DETECTION

In this section we demonstrate the flexibility of DCT bases for non-classification related task, namely object contour regression. The challenge here is to distinguish meaningful edges from edges representing a texture. Data and annotations are provided by the Berkeley Segmentation Data Set and Benchmarks (BSDS500) [70]. Our model is built on top of Holistically Nested Edge Detection (HED) [71], which is based on VGG16 network [49]. This model learns multi-scale representations, and at each scale a boundary is predicted as a linear combination of the features at the deepest layer in that scale. Predictions generated from the subsampled features are upsampled with bilinear interpolation to match the ground truth resolution. The final prediction is estimated as a weighted average of all the side outputs. A cross-entropy between each side output and the ground truth contributes to the loss function. Following Xie et al. [71], annotations from different annotators are merged based on majority vote. Images are augmented into 3 scales, 16 rotations and two horizontally mirrored versions. Training is performed with Adaptive Momentum Optimizer.

Overlap of the predictions with human annotations is measured as an F-score on a precision-recall curve. Two metrics are standardly reported on this dataset: the Optimal Dataset Scale (ODS) using fixed contour threshold, and the Optimal Image Scale (OIS) that is calculated selecting image-best thresholds. Following [71], edges are thinned with non-maximum suppression prior to evaluation. Our re-implementation of HED with random weight initialization scores 0.761 ODS and 0.778 OIS (see HED in Tab. 14). Replacing all the filters with harmonic blocks based on Alg. 1 improves both metrics: ODS to 0.770, and OIS to 0.789 (see Harm-HED in Tab. 14). The qualitative comparison presented in Fig. 10 demonstrates how the Harmonic version of HED handles better the suppression of texture-related edges preserving the relevant object boundaries. Initialization with a

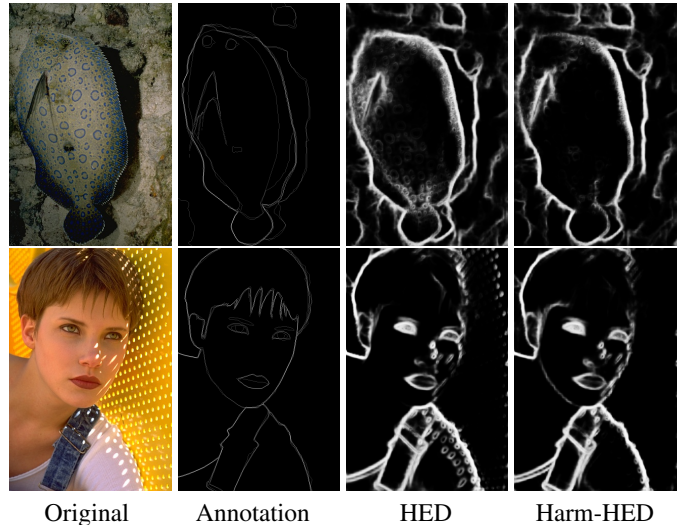


Fig. 10. Qualitative results of harmonic HED model trained from randomly initialized weights. Our approach (Harm-HED) is better at suppressing texture-imposed edges.

pretrained model typically plays an important role in this task. The quantitative comparison is repeated after initializing weights using the VGG16 weights learned on Imagenet. Harmonic HED was initialized by the same set of weights using the network conversion to DCT bases. This initialization provided a minor gain in performance, still falling behind the results reported by [71], see scores in Table 14. Interestingly, our harmonic HED still reaches better performance even when both models are initialized the same way.

Moreover, comparisons with two recent works based on steerable filters for boundary detection are included. First, locally adaptive filtering for boundary detection was employed using a shallow residual network with dynamic steerable blocks [72]. These blocks leverage steering properties of Gaussian derivative bases which linearize certain transformations. Second, Worrall et al. [28] have modified HED architecture with complex circular harmonic bases to detect boundaries via representations equivariant to rotations. Both of these implementations use notably smaller models. To match these we downscale our Harmonic HED architectures by limiting the number of channels and network depth similarly to [28]. Using DCT bases slightly improves the small baseline model that already performs reasonably well, see

TABLE 14

Boundary detection results measured by ODS and OIS (higher is better). Our proposed models are denoted as Harm-HED.

Method	Layers/Chan.	Params	ODS	OIS
<b>Random initialization</b>				
HED	13 / 64	14 626k	0.761	0.778
Harm-HED	13 / 64	14 626k	<b>0.770</b>	<b>0.789</b>
HED	10 / 7	113k	0.738	0.756
Harm-HED	10 / 7	113k	0.743	0.763
Harm-HED $\lambda=2$	10 / 7	38k	0.740	0.758
Harm-HED progr. $\lambda$	10 / 10	118k	0.751	0.770
H-Net [28]	10 / -	116k	0.726*	0.742*
DynResNet [72]	-	-	0.732*	0.751*
<b>Pretrained</b>				
HED	13 / 64	14 626k	0.777	0.796
Harm-HED	13 / 64	14 626k	0.782	0.803
HED [71]	13 / 64	14 626k	0.790*	0.808*

\*scores reported by the authors of the corresponding papers.

Tab. 14. Note, that different hyperparameters have been used to train these harmonic nets. Equivariant harmonic network [28] has complex bases that require complex convolution and learning parameters for imaginary components as well. Increasing the number of channels (from 7 to 10) in our Harmonic HED while using progressive compression leads to a model with comparable number of parameters yet better performance due to more rich feature space. We observe that our ‘static’ approach based on DCT bases without explicitly built-in invariance can detect boundaries well compared to becnhmark methods.

## 7 CONCLUSION

We have presented a novel approach to explicitly incorporate spectral information from DCT into CNN models. We have empirically evaluated the use of our harmonic blocks with the well-established state-of-the-art CNN architectures, and shown that our approach improves results (e.g. accuracy & complexity) for a range of applications including image classification, segmentation and boundary detection. We also ascertain that harmonic networks can be efficiently set-up by converting the pretrained CNN baselines. The use of DCT allows one to order the harmonic block parameters by their significance from the most relevant low frequency to less important high frequencies. This enables efficient model compression by parameter truncation with only minor degradation in the model performance. This has been shown to be particularly useful for tasks with limited training samples [6].

## ACKNOWLEDGEMENTS

This research was supported by the ADAPT Centre for Digital Content Technology funded under the SFI Research Centres Programme (Grant 13/RC/2106) and co-funded under the European Regional Development Fund. We gratefully acknowledge the support of NVIDIA Corporation with the donation of the Titan Xp GPUs.

## REFERENCES

- [1] Joan Bruna and Stéphane Mallat. Invariant scattering convolution networks. *IEEE Trans. Pat. Anal. Mach. Intel.*, 35(8):1872–1886, 2013.
- [2] Gregory K Wallace. The jpeg still picture compression standard. *IEEE transactions on consumer electronics*, 38(1):xviii–xxxiv, 1992.
- [3] Qiang Qiu, Xiuyuan Cheng, Robert Calderbank, and Guillermo Sapiro. DCFNet: Deep neural network with decomposed convolutional filters. In *Proc. of the 35th International Conference on Machine Learning*, volume 80, pages 4198–4207. PMLR, Jul 2018.
- [4] Muhammad Tayyab and Abhijit Mahalanobis. Basisconv: A method for compressed representation and learning in cnns. *arXiv preprint arXiv:1906.04509*, 2019.
- [5] Matej Ulicny, Vladimir A Krylov, and Rozenn Dahyot. Harmonic networks for image classification. In *Proc. of British Machine Vision Conference (BMVC)*, Sep. 2019.
- [6] Matej Ulicny, Vladimir A Krylov, and Rozenn Dahyot. Harmonic networks with limited training samples. In *European Signal Processing Conference (EUSIPCO)*, Sep. 2019.
- [7] Qing Wang and Rong Zhang. Double JPEG compression forensics based on a convolutional neural network. *EURASIP J. on Information Security*, 2016(1):23, Oct 2016.
- [8] I. Amerini, T. Uricchio, L. Ballan, and R. Caldelli. Localization of JPEG double compression through multi-domain convolutional neural networks. In *2017 IEEE Conference on Computer Vision and Pattern Recognition Workshops (CVPRW)*, pages 1865–1871, July 2017.
- [9] M. Barni, L. Bondi, N. Bonettini, P. Bestagini, A. Costanzo, M. Maggini, B. Tondi, and S. Tubaro. Aligned and non-aligned double JPEG detection using convolutional neural networks. *J. Vis. Comun. Image Represent.*, 49(C):153–163, November 2017.
- [10] Bin Li, Haoxin Zhang, Hu Luo, and Shunquan Tan. Detecting double jpeg compression and its related anti-forensic operations with cnn. *Multimedia Tools and Applications*, 78(7):8577–8601, 2019.
- [11] Xiaoyi Zou, Xiangmin Xu, Chunmei Qing, and Xiaofen Xing. High speed deep networks based on discrete cosine transformation. In *Image Processing (ICIP), 2014 IEEE International Conference on*, pages 5921–5925. IEEE, 2014.
- [12] Meng Joo Er, W. Chen, and Shiqian Wu. High-speed face recognition based on discrete cosine transform and rbf neural networks. *Trans. Neur. Netw.*, 16(3):679–691, May 2005.
- [13] A. Ghosh and R. Chellappa. Deep feature extraction in the DCT domain. In *2016 23rd International Conference on Pattern Recognition (ICPR)*, pages 3536–3541, Dec 2016.
- [14] Matej Ulicny and Rozenn Dahyot. On using CNN with DCT based image data. In *Irish Machine Vision and Image Processing Conference*, 2017.
- [15] Lionel Gueguen, Alex Sergeev, Ben Kadlec, Rosanne Liu, and Jason Yosinski. Faster neural networks straight from JPEG. In *Advances in Neural Information Processing Systems*, pages 3933–3944, 2018.
- [16] Edouard Oyallon and Stéphane Mallat. Deep roto-translation scattering for object classification. In *Conf. on Computer Vision and Pattern Recognition (CVPR)*, June 2015.
- [17] E. Oyallon, S. Zagoruyko, G. Huang, N. Komodakis, S. Lacoste-Julien, M. Blaschko, and E. Belilovsky. Scattering networks for hybrid representation learning. *IEEE Transactions on Pattern Analysis and Machine Intelligence*, 41(9):2208–2221, Sep. 2019.
- [18] Amarjot Singh and Nick Kingsbury. Efficient convolutional network learning using parametric log based dual-tree wavelet scatternet. In *Computer Vision Workshop (ICCVW), 2017 IEEE International Conference on*, pages 1140–1147. IEEE, 2017.
- [19] Edouard Oyallon, Eugene Belilovsky, Sergey Zagoruyko, and Michal Valko. Compressing the input for CNNs with the first-order scattering transform. In *European Conference on Computer Vision (ECCV)*, 2018.
- [20] T. Williams and R. Li. Advanced image classification using wavelets and convolutional neural networks. In *2016 15th IEEE International Conference on Machine Learning and Applications (ICMLA)*, pages 233–239, Dec 2016.
- [21] S. Said, O. Jemai, S. Hassairi, R. Ejbal, M. Zaied, and C. Ben Amar. Deep wavelet network for image classification. In *2016 IEEE International Conference on Systems, Man, and Cybernetics*, pages 922–927, Oct 2016.
- [22] D. D. N. De Silva, S Fernando, I. T. S. Piyatilake, and A. V. S Karunaratne. Wavelet based edge feature enhancement for convolutional neural networks. In *Eleventh International Conference on Machine Vision (ICMV 2018)*, volume 11041, page 110412R. International Society for Optics and Photonics, 2019.
- [23] Travis Williams and Robert Li. Wavelet pooling for convolutional neural networks. In *International Conference on Learning Representations (ICLR)*, 2018.
- [24] Oren Rippel, Jasper Snoek, and Ryan P Adams. Spectral representations for convolutional neural networks. In *Advances in neural information processing systems*, pages 2449–2457, 2015.
- [25] Shin Fujieda, Kohei Takayama, and Toshiya Hachisuka. Wavelet convolutional neural networks for texture classification. *arXiv preprint arXiv:1707.07394*, 2017.
- [26] H. Lu, H. Wang, Q. Zhang, D. Won, and S. W. Yoon. A dual-tree complex wavelet transform based convolutional neural network for human thyroid medical image segmentation. In *2018 IEEE International Conference on Healthcare Informatics (ICHI)*, pages 191–198, June 2018.
- [27] Shangzhen Luan, Chen Chen, Baochang Zhang, Jungong Han, and Jianzhuang Liu. Gabor convolutional networks. *IEEE Trans. Image Process.*, 27(9):4357–4366, 2018.
- [28] Daniel E Worrall, Stephan J Garbin, Daniyar Turmukhambetov, and Gabriel J Brostow. Harmonic networks: Deep translation and rotation equivariance. In *Conf. on Computer Vision and Pattern Recognition (CVPR)*, pages 5028–5037, 2017.
- [29] Jorn-Henrik Jacobsen, Jan van Gemert, Zhongyu Lou, and Arnold WM Smeulders. Structured receptive fields in CNNs. In *Conf. on Computer Vision and Pattern Recognition (CVPR)*, pages 2610–2619, 2016.
- [30] Takumi Kobayashi. Analyzing filters toward efficient convnet. In *Proceedings of the IEEE Conference on Computer Vision and Pattern Recognition*, pages 5619–5628, 2018.
- [31] Max Jaderberg, Andrea Vedaldi, and Andrew Zisserman. Speeding up convolutional neural networks with low rank expansions. In *British Machine Vision Conference (BMVC)*. BMVA Press, 2014.
- [32] Wenlin Chen, James Wilson, Stephen Tyree, Kilian Q. Weinberger, and Yixin Chen. Compressing convolutional neural networks in the frequency domain. In *Proc. of the 22Nd ACM SIGKDD International Conference*



- on *Knowledge Discovery and Data Mining*, KDD '16, pages 1475–1484, New York, NY, USA, 2016. ACM.
- [33] Yunhe Wang, Chang Xu, Shan You, Dacheng Tao, and Chao Xu. CN-Npack: Packing convolutional neural networks in the frequency domain. In D. D. Lee, M. Sugiyama, U. V. Luxburg, I. Guyon, and R. Garnett, editors, *Advances in Neural Information Processing Systems* 29, pages 253–261. Curran Associates, Inc., 2016.
  - [34] Song Han, Huizi Mao, and William J Dally. Deep compression: Compressing deep neural networks with pruning, trained quantization and Huffman coding. *International Conference on Learning Representations (ICLR)*, 2016.
  - [35] Minyoung Kim and Luca Rigazio. Deep clustered convolutional kernels. In *Feature Extraction: Modern Questions and Challenges*, pages 160–172, 2015.
  - [36] Rafael C. Gonzalez and Richard E. Woods. *Digital Image Processing*. Prentice Hall, Upper Saddle River, N.J., 3rd edition, 2008.
  - [37] Ruyue Wang. *Introduction to orthogonal transforms: with applications in data processing and analysis*. Cambridge University Press, 2012.
  - [38] H. S. Malvar. Lapped transforms for efficient transform/subband coding. *IEEE Transactions on Acoustics, Speech, and Signal Processing*, 38(6):969–978, June 1990.
  - [39] Kaiming He, Xiangyu Zhang, Shaoqing Ren, and Jian Sun. Deep residual learning for image recognition. In *Conf. on Computer Vision and Pattern Recognition (CVPR)*, pages 770–778, 2016.
  - [40] Sergey Zagoruyko and Nikos Komodakis. Wide residual networks. In Edwin R. Hancock Richard C. Wilson and William A. P. Smith, editors, *Proc. of British Machine Vision Conference (BMVC)*, pages 87.1–87.12. BMVA Press, September 2016.
  - [41] Yann LeCun, Fu Jie Huang, and Leon Bottou. Learning methods for generic object recognition with invariance to pose and lighting. In *Computer Vision and Pattern Recognition, 2004. CVPR 2004. Proc. of the 2004 IEEE Computer Society Conference on*, volume 2, pages II–104. IEEE, 2004.
  - [42] Geoffrey E Hinton, Sara Sabour, and Nicholas Frosst. Matrix capsules with EM routing. In *International Conference on Learning Representations*, 2018.
  - [43] Dan C Ciresan, Ueli Meier, Jonathan Masci, Luca Maria Gambardella, and Jürgen Schmidhuber. Flexible, high performance convolutional neural networks for image classification. In *IJCAI Proc.-International Joint Conference on Artificial Intelligence*, volume 22, page 1237. Barcelona, Spain, 2011.
  - [44] E. M. Rehn and H. Sprekeler. Nonlinear supervised locality preserving projections for visual pattern discrimination. In *2014 22nd International Conference on Pattern Recognition*, pages 1568–1573, Aug 2014.
  - [45] Alex Krizhevsky et al. Learning multiple layers of features from tiny images. Technical report, Citeseer, 2009.
  - [46] Torchvision models. <https://pytorch.org/docs/stable/torchvision/models.html>.
  - [47] Sam Gross and Michael Wilber. Training and investigating residual nets. *Facebook AI Research*, 2016.
  - [48] Christian Szegedy, Wei Liu, Yangqing Jia, Pierre Sermanet, Scott Reed, Dragomir Anguelov, Dumitru Erhan, Vincent Vanhoucke, and Andrew Rabinovich. Going deeper with convolutions. In *Conf. on Computer Vision and Pattern Recognition (CVPR)*, pages 1–9, 2015.
  - [49] Karen Simonyan and Andrew Zisserman. Very deep convolutional networks for large-scale image recognition. *arXiv preprint:1409.1556*, 2014.
  - [50] Saining Xie, Ross Girshick, Piotr Dollár, Zhuowen Tu, and Kaiming He. Aggregated residual transformations for deep neural networks. In *Proceedings of the IEEE conference on computer vision and pattern recognition*, pages 1492–1500, 2017.
  - [51] J. Hu, L. Shen, S. Albanie, G. Sun, and E. Wu. Squeeze-and-excitation networks. *IEEE Transactions on Pattern Analysis and Machine Intelligence*, pages 1–1, 2019.
  - [52] Xingcheng Zhang, Zhizhong Li, Chen Change Loy, and Dahua Lin. Polynet: A pursuit of structural diversity in very deep networks. In *Proceedings of the IEEE Conference on Computer Vision and Pattern Recognition*, pages 718–726, 2017.
  - [53] Yunpeng Chen, Jianan Li, Huaxin Xiao, Xiaojie Jin, Shuicheng Yan, and Jiashi Feng. Dual path networks. In *Advances in Neural Information Processing Systems*, pages 4467–4475, 2017.
  - [54] Mingxing Tan and Quoc Le. EfficientNet: Rethinking model scaling for convolutional neural networks. In Kamalika Chaudhuri and Ruslan Salakhutdinov, editors, *Proceedings of the 36th International Conference on Machine Learning*, volume 97 of *Proceedings of Machine Learning Research*, pages 6105–6114, Long Beach, California, USA, 09–15 Jun 2019. PMLR.
  - [55] Barret Zoph, Vijay Vasudevan, Jonathon Shlens, and Quoc V Le. Learning transferable architectures for scalable image recognition. In *Proceedings of the IEEE conference on computer vision and pattern recognition*, pages 8697–8710, 2018.
  - [56] Esteban Real, Alok Aggarwal, Yanping Huang, and Quoc V Le. Regularized evolution for image classifier architecture search. In *Proceedings of the AAAI Conference on Artificial Intelligence*, volume 33, pages 4780–4789, 2019.
  - [57] Chenxi Liu, Barret Zoph, Maxim Neumann, Jonathon Shlens, Wei Hua, Li-Jia Li, Li Fei-Fei, Alan Yuille, Jonathan Huang, and Kevin Murphy. Progressive neural architecture search. In *Proceedings of the European Conference on Computer Vision (ECCV)*, pages 19–34, 2018.
  - [58] Gao Huang, Yu Sun, Zhuang Liu, Daniel Sedra, and Kilian Q Weinberger. Deep networks with stochastic depth. In *European conference on computer vision*, pages 646–661. Springer, 2016.
  - [59] Ilya Loshchilov and Frank Hutter. Sgdr: Stochastic gradient descent with warm restarts. In *International Conference on Learning Representations*, 2017.
  - [60] Zhun Zhong, Liang Zheng, Guoliang Kang, Shaozi Li, and Yi Yang. Random erasing data augmentation. *arXiv preprint arXiv:1708.04896*, 2017.
  - [61] Tsung-Yi Lin, Priya Goyal, Ross Girshick, Kaiming He, and Piotr Dollár. Focal loss for dense object detection. In *Proc. of the IEEE international conference on computer vision*, pages 2980–2988, 2017.
  - [62] Shaoqing Ren, Kaiming He, Ross Girshick, and Jian Sun. Faster r-cnn: Towards real-time object detection with region proposal networks. In *Advances in neural information processing systems*, pages 91–99, 2015.
  - [63] Kaiming He, Georgia Gkioxari, Piotr Dollár, and Ross Girshick. Mask r-cnn. In *Proc. of the IEEE international conference on computer vision*, pages 2961–2969, 2017.
  - [64] Mark Everingham, Luc Van Gool, Christopher KI Williams, John Winn, and Andrew Zisserman. The pascal visual object classes (voc) challenge. *International journal of computer vision*, 88(2):303–338, 2010.
  - [65] Tsung-Yi Lin, Michael Maire, Serge Belongie, James Hays, Pietro Perona, Deva Ramanan, Piotr Dollár, and C Lawrence Zitnick. Microsoft coco: Common objects in context. In *European conference on computer vision*, pages 740–755. Springer, 2014.
  - [66] Kai Chen, Jiaqi Wang, Jiangmiao Pang, Yuhang Cao, Yu Xiong, Xiaoxiao Li, Shuyang Sun, Wansen Feng, Ziwei Liu, Jiarui Xu, Zheng Zhang, Dazhi Cheng, Chenchen Zhu, Tianheng Cheng, Qijie Zhao, Buyu Li, Xin Lu, Rui Zhu, Yue Wu, Jifeng Dai, Jingdong Wang, Jianping Shi, Wanli Ouyang, Chen Change Loy, and Dahua Lin. Mmdetection: Open mmlab detection toolbox and benchmark. *CoRR*, abs/1906.07155, 2019.
  - [67] Tsung-Yi Lin, Piotr Dollár, Ross Girshick, Kaiming He, Bharath Hariharan, and Serge Belongie. Feature pyramid networks for object detection. In *Proc. of the IEEE conference on computer vision and pattern recognition*, pages 2117–2125, 2017.
  - [68] Zhaowei Cai and Nuno Vasconcelos. Cascade r-cnn: Delving into high quality object detection. In *Proc. of the IEEE conference on computer vision and pattern recognition*, pages 6154–6162, 2018.
  - [69] K. Chen, J. Pang, J. Wang, Y. Xiong, X. Li, S. Sun, W. Feng, Z. Liu, J. Shi, W. Ouyang, C. C. Loy, and D. Lin. Hybrid task cascade for instance segmentation. In *2019 IEEE/CVF Conference on Computer Vision and Pattern Recognition (CVPR)*, pages 4969–4978, June 2019.
  - [70] Pablo Arbelaez, Michael Maire, Charles Fowlkes, and Jitendra Malik. Contour detection and hierarchical image segmentation. *IEEE Trans. Pattern Anal. Mach. Intell.*, 33(5):898–916, May 2011.
  - [71] Saining Xie and Zhuowen Tu. Holistically-nested edge detection. In *Proceedings of the IEEE international conference on computer vision*, pages 1395–1403, 2015.
  - [72] Jorn-Henrik Jacobsen, Bert De Brabandere, and Arnold Smeulders. Dynamic steerable blocks in deep residual networks. In Gabriel Brostow Tae-Kyun Kim, Stefanos Zafeiriou and Krystian Mikolajczyk, editors, *Proceedings of the British Machine Vision Conference (BMVC)*, pages 145.1–145.13. BMVA Press, September 2017.